Electrogram Fractionation

The Relationship Between Spatiotemporal Variation of Tissue Excitation and Electrode Spatial Resolution

Daniel D. Correa de Sa, MD; Nathaniel Thompson, MD; Justin Stinnett-Donnelly, MD; Pierre Znojkiewicz, MD; Nicole Habel; Joachim G. Müller, MD; Jason H.T. Bates, PhD; Jeffrey S. Buzas, PhD; Peter S. Spector, MD

Background—Fractionated electrograms are used by some as targets for ablation in atrial and ventricular arrhythmias. Fractionation has been demonstrated to result when there is repetitive or asynchronous activation of separate groups of cells within the recording region of a mapping electrode(s).

Methods and Results—Using a computer model, we generated tissue activation patterns with increasing spatiotemporal variation and calculated virtual electrograms from electrodes with decreasing resolution. We then quantified electrogram fractionation. In addition, we recorded unipolar electrograms during atrial fibrillation in 20 patients undergoing atrial fibrillation ablation. From these we constructed bipolar electrograms with increasing interelectrode spacing and quantified fractionation. During modeling of spatiotemporal variation, fractionation varied directly with electrode length, diameter, height, and interelectrode spacing. When resolution was held constant, fractionation increased with increasing spatiotemporal variation. In the absence of spatial variation, fractionation was independent of resolution and proportional to excitation frequency. In patients with atrial fibrillation, fractionation increased as interelectrode spacing increased.

Conclusions—We created a model for distinguishing the roles of spatial and temporal electric variation and electrode resolution in producing electrogram fractionation. Spatial resolution affects fractionation attributable to spatiotemporal variation but not temporal variation alone. Electrogram fractionation was directly proportional to spatiotemporal variation and inversely proportional to spatial resolution. Spatial resolution limits the ability to distinguish high-frequency excitation from overcounting. In patients with atrial fibrillation, complex fractionated atrial electrogram detection varies with spatial resolution. Electrode resolution must therefore be considered when interpreting and comparing studies of fractionation. **(*Circ Arrhythm Electrophysiol*. 2011;4:909-916.)**

Key Words: CFAE ■ electrogram ■ fractionation ■ mapping ■ spatial resolution

Fractionated electrograms have attracted the attention of clinical electrophysiologists in the setting of mapping re-entrant rhythms (eg, ventricular and atrial tachycardia) and more recently mapping of atrial fibrillation. Fractionation in these settings is felt to identify substrate relevant to the arrhythmia circuitry. Although fractionation can identify a critical isthmus in scar-based reentrant ventricular tachycardia circuits,[1,2] the use of fractionated electrograms to guide atrial fibrillation ablation has had conflicting results. Despite the initial successes reported by Nademanne et al,[3] subsequent studies have led to mixed results.[4–9]

Clinical Perspective on p 916

Although there is no uniformly accepted definition, the term "complex fractionated atrial electrograms" has been used to describe electrograms with low amplitude and high-frequency deflections. Electrograms measure the changing potential field at the site of a recording electrode.[10] Any pattern of tissue activation within the recording region of an electrode that results in alternation between increasing and decreasing potential will produce electrogram fractionation. Several disparate tissue activation patterns have been shown to result in electrogram fractionation, including meandering rotors,[11,12] wave collision,[11] discontinuous conduction,[13,14] and longitudinal dissociation.[15,16] Using monophasic action potential recordings in patients with atrial fibrillation, Narayan et al have also demonstrated that complex fractionated atrial electrograms can have multiple etiologies.[17] Because of their nonunique relationship (activation and electrogram), one cannot unambiguously determine a specific tissue

Received June 7, 2011; final revision received September 14, 2011; accepted September 20, 2011.

From the Department of Medicine (D.D.C., N.T., J.S.-D., P.Z., N.H., J.G.M., J.H.T.B., P.S.S.), University of Vermont College of Medicine, Burlington, VT; Fletcher Allen Health Care (D.D.C., N.T., J.S.-D., P.Z., N.H., J.G.M., J.H.T.B., P.S.S.), Burlington, VT; the College of Engineering and Mathematical Sciences (J.H.T.B., J.S.B.), University of Vermont, Burlington, VT; and the Cardiovascular Research Institute (J.H.T.B., P.S.S.), Burlington, VT.

The online-only Data Supplement is available at http://circep.ahajournals.org/lookup/suppl/doi:10.1161/CIRCEP.111.965145/-/DC1.

Correspondence to Peter S. Spector, MD, McClure 1 Cardiology, 111 Colchester Avenue, Burlington, VT 05401. E-mail peter.spector@uvm.edu.

Circ Arrhythm Electrophysiol **is available at http://circep.ahajournals.org** **DOI: 10.1161/CIRCEP.111.965145**

activation pattern based solely on the observation of fractionation.

Because fractionation results from tissue dyssynchrony within the electrode recording region, it follows that the area of tissue that contributes to the electrogram will influence fractionation. Spatial resolution refers to the area of tissue that contributes to the electrogram. Because tissue currents create a potential field that spreads infinitely through space, the "area that contributes to the electrogram" is in fact infinite. However, because potential decreases with distance from a current source, the effective area that contributes to an electrogram is small and varies with electrode size (length and diameter), configuration (unipolar versus bipolar), height above the tissue, and interelectrode spacing (IES).[18]

In a series of studies using a computer model of excitable tissue and electrogram recordings from patients with atrial fibrillation, we defined the components that produce electrogram fractionation. We hypothesized that electrogram fractionation can result from either (1) spatiotemporal variation of tissue electric activity; or (2) from temporal variation alone; and that the former (overcounting) is dependent on electrode spatial resolution, whereas the latter (rapid repetitive excitation) is not.

Methods

Modeling Studies

We studied activation in a 2-dimensional sheet of electrically excitable tissue using a computer model. We calculated the surrounding potential field produced by tissue excitation. With the model we were able to independently vary the temporal and spatiotemporal complexity of tissue excitation. By recording from virtual electrodes of varied size, configuration, and height, we quantified the impact of spatial resolution on fractionation.

Computer Model Design

The model design has been described in detail previously.[19] Briefly, the model is a monodomain cellular automaton; cells are arranged in a 2-dimensional grid with each cell connected to its 4 neighbors (up, down, left, and right). Cell voltage changes in response to an action potential, external stimulation, or intercellular current flow. The membrane voltage of a cell corresponds to its level of electric depolarization. The resting state of a cell corresponds to quiescence. As a cell gathers current membrane voltage depolarizes, when membrane voltage exceeds voltage threshold, an action potential is initiated. Action potential upstroke velocity and action potential duration are rate- and voltage-dependent conferring restitution as described previously.[19] Cells connect to their immediate neighbors through electrically resistive pathways. The vertical and horizontal resistive constants are R_v and R_h, respectively. Cells exchange current with their neighbors according to first-order kinetics, whereby the voltage of a quiescent cell (j, k) at time t is affected by that of its neighbors according to

$$(1)\quad \frac{dV(j,k,t)}{dt} = \frac{1}{R_h}[V(j-1,k,t)+V(j+1,k,t)-2V(j,k,t)] + \frac{1}{R_v}[V(j,k-1,t)+V(j,k+1,t)-2V(j,k,t)]$$

At each time step in the simulation, all cells have their values of membrane voltage updated according to

$$(2)\quad V(j,k,t)=V(j,k,t-1)+\frac{dV(j,k,t)}{dt}\delta t + V\text{intrinsic}$$

where δt is the time step size. A cell may be defined as scar, in which case it is permanently quiescent and electrically isolated from its neighbors.

Tissue Variability

In a flat square sheet of tissue 1 cell thick (10×10 mm) without anisotropy, we introduce temporal variation by modulating excitation frequency. Activation wave fronts propagate through the homogeneous tissue at constant conduction velocity.

Spatial variation is created by adding parallel lines of scar alternately extending to the top or bottom edge of the tissue (Figure 1; Supplemental Video; http://circ.ahajournals.org). Spatiotemporal variation is then introduced by stimulating in the upper left corner; activation waves proceed through the tissue with a "zig-zag" pattern.

Two components of tissue activation complexity can then be independently manipulated: (1) temporal variation can be modulated by changing activation frequency; and (2) spatiotemporal complexity can be increased by increasing the number of parallel lines of scar; that is, increasing the number of separate tissue bundles through which excitation spreads.

Extracellular Potential Recordings

We calculate the potential, $\Phi(m, n, t)$, that would be recorded by an electrode placed at a height h above a site in the tissue plane (m, n) at each time (t). In the context of the monodomain approximation used, each cell in the tissue makes a contribution to the electrogram that is proportional to the cell's transmembrane current and inversely proportional to its linear distance from the electrode.[20] We assume that the transmembrane current at a particular cell is the time-derivative of voltage (V), approximated as the difference in V between successive time steps. That is,

$$(3)\quad \Phi(m,n,t)=\sum_{j=1}^{n}\sum_{k=1}^{n}\frac{V(j,k,t)-V(j,k,t-1)}{\sqrt{(j-m)^2+(k-n)^2+h^2}}$$

where j and k are position indices in the x and y directions.

Virtual Electrograms

We modeled 3-dimensional cylindrical electrodes and varied length, diameter, and height (Figure 2). The electrodes were modeled as hollow cylinders divided into a finite element mesh with elements evenly distributed about the circumference and along the length of the electrode. The number of elements varied depending on electrode geometry so no element area was >1 mm^2. Using Eq 3, the electric potential contribution from each cell was calculated at the center of each element. The potential recorded by the entire unipolar electrode was then calculated as the sum of each element potential multiplied by the element area and divided by the total surface area of the electrode. The bipolar electrogram was obtained simply as the difference in the potentials recorded by the 2 unipolar electrodes. Height was measured from the tissue to the electrode's bottom edge and, for bipolar recording, IES was measured between edges. Electrodes were positioned over the center of the tissue (perpendicular to lines of scar—unipolar; parallel to lines of scar—bipolar recordings).

Electrode spatial resolution varies inversely with electrode surface area (length and diameter), height above tissue, and IES (for bipolar recordings).

Electrogram Analysis

The cellular automaton model evolves through discrete time steps; as a result, electrogram amplitude fluctuates from time step to time step. The electrogram signal was therefore processed with a smoothing function to reduce this artifact. We quantified the number of turning

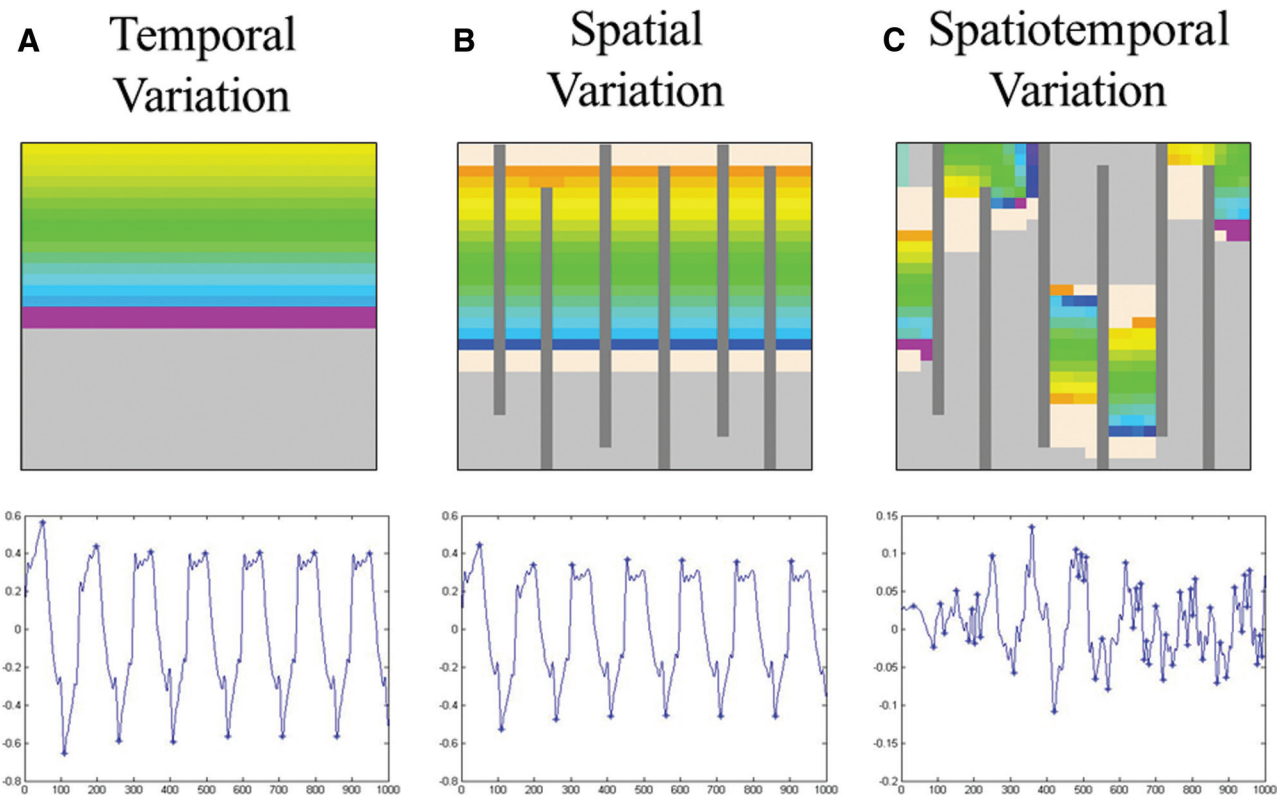

Figure 1. Simulation of temporal, spatial, and spatiotemporal variation of tissue excitation. **Top row**, Tissue voltage distribution (single time step; 10×10 mm). **A**, Temporal variation: stimulation of the top row of cells (cycle length 150 ms) produced sequential planar waves of excitation. **B**, Spatial variation: although tissue is divided by multiple alternating linear scars, activation proceeds from top to bottom in parallel (secondary to simultaneous stimulation of the top row of cells). **C**, Spatiotemporal variation: stimulation from the top left corner results in sequential excitation of vertical channels between linear scars, producing "zig-zag" activation waves every 150 ms. **Bottom row**, Corresponding virtual unipolar electrograms (electrode diameter 1 mm, height 0.5 mm, length 6 mm, oriented horizontally). Turning points are marked with stars. Note that even with linear scars, if activation occurs simultaneously in all bundles, the electrogram is very similar to that seen with in tissue without scar (**A** versus **B**). The contributions of each bundle to the potential field occur simultaneously and are hence superimposed in the electrogram (no fractionation).

points as the number of peaks and troughs with a 10% tolerance as previously described.[21,22]

Nomenclature Clarification

In this study, temporal variation refers to spatially coordinated changes in the frequency of activation and spatiotemporal variability refers to asymmetrical excitation of various tissue sites in time.

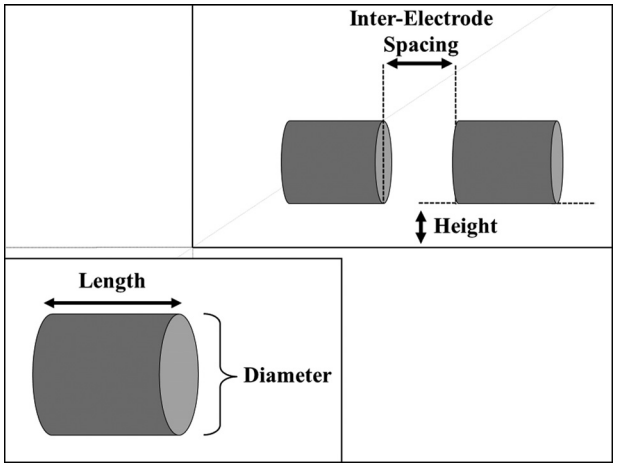

Figure 2. Electrode geometry. Electrode geometry (inset lower left), spacing, and position.

Clinical Studies

We obtained 2 60-second unipolar recordings during atrial fibrillation (AF) from the coronary sinus of 20 patients presenting for AF ablation. Average patient age was 59±7 years; 9 patients had paroxysmal and 11 had persistent AF. Unipolar electrograms (indifferent electrode in the inferior vena cava (length=diameter=2 mm; Bard Electrophysiology, Billerica, MA) were recorded with either a 20-pole (1 mm electrodes, 1-3-1–mm spacing; 10 patients) or a 10-pole (2-mm electrodes, 2-5-2–mm spacing; 10 patients) catheter (Biosense Webster, Diamond Bar, CA). Signals (sampled at 1 kHz, filtered 30–250 Hz) were exported for offline analysis. From these we constructed bipolar electrograms with increasing interelectrode spacing (electrodes 1–2, 1–3, and 1–4). Bipolar signals were analyzed using standard algorithms for average interpotential interval (AIPI) and interval confidence level (ICL).[23] The voltage window for ICL was 0.05 to 0.2 mV; the upper limit of 0.2 mV was selected as an average of values used by different groups.[24,25] The amplitude of electromagnetic noise in each signal was measured in 10 patients (during sinus rhythm). The study was approved by the Institutional Review Committee on Human Research.

Statistical Methods

We used a mixed effects linear model for the analysis of the experimental data for studying fractionation as a function of interelectrode spacing. Data for each catheter type and each outcome (ICL and AIPI) were analyzed separately. Subjects within a catheter type were treated as random effects, thereby inducing a compound-symmetrical correlation structure among within-subject measurements. Measurements between subjects were

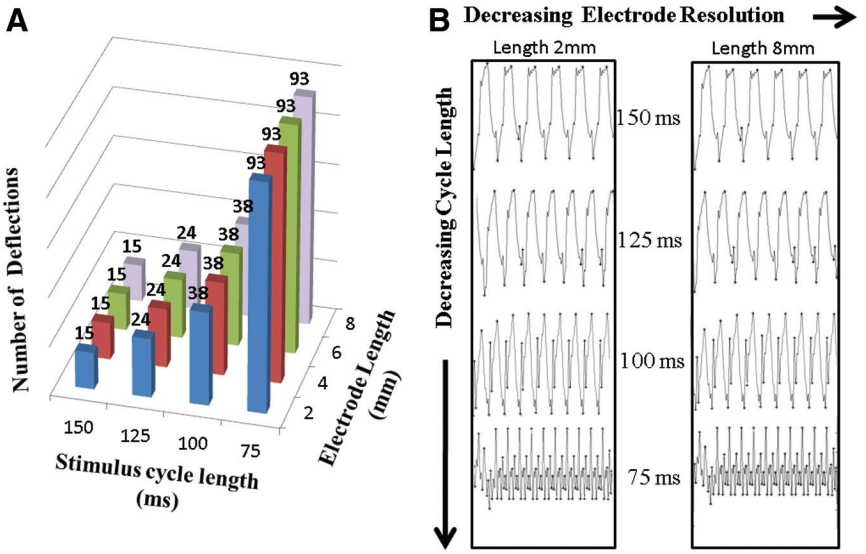

Figure 3. Temporal variation: electrogram fractionation is independent of electrode resolution. In a homogeneous sheet of tissue (no linear scar) with planar activation, the number of deflections in the unipolar electrogram was measured at the time of varying cycle length and electrode length. **A**, Number of deflections versus stimulus cycle length; electrode length 2, 4, 6, and 8 mm (diameter 1 mm, height 0.5 mm). **B**, Examples of virtual unipolar electrograms from tissue excited at decreasing cycle lengths: cycle length 150 ms (top) to 75 ms (bottom), recorded with a unipolar electrode of 2 mm (left) and 8 mm (right) in length. Note that number of deflections is independent of electrode size.

independent. IES and time of measurement were treated as fixed effects with time of measurement nested within subject. Analysis was done using PROC MIXED in SAS, Version 9.3.

Results

Modeling Studies

Fractionation as a Function of Temporal Variation

In a series of simulations we stimulated tissue (without linear scars) at progressively shorter cycle lengths (150, 125, 100, and 75 ms). Virtual electrograms were recorded using unipolar electrodes (6-mm length, 1-mm diameter, and 0.5-mm height). Fractionation was directly proportional to tissue frequency; 15, 24, 38, and 93 deflections at cycle lengths of 150, 125, 100, and 75 ms, respectively (Figure 3).

Impact of Electrode Spatial Resolution—Temporal Variation

With temporal variation alone, fractionation was independent of electrode spatial resolution (Figure 3). In tissue without scars stimulated at 150-ms cycle length, the number of deflections in the unipolar electrogram was independent of electrode length, diameter, or height (15 deflections for electrode length 2, 4, 6, and 8 mm; diameter 1, 2, 3, and 4 mm; height 0.5, 1, 2, and 3 mm). Bipolar recordings (1-mm length and diameter, 0.5-mm height) had 27 deflections regardless of IES (1, 3, 5, and 7 mm).

Fractionation as a Function of Spatiotemporal Variation

To create spatiotemporal variation, tissue was stimulated at a fixed cycle length of 150 ms from the upper left corner resulting in a "zig-zag" activation pattern. When electrode spatial resolution was kept constant, fractionation was directly proportional to the number of linear scars (ie, spatiotemporal complexity); the number of deflections was 19, 26, 45, and 52 for tissue with 1, 2, 4, and 6 lines of scar, respectively (unipolar 6-mm length, 1-mm diameter, and 0.5-mm height; Figure 4). With bipolar recordings (1-mm length and diameter, 0.5-mm height, and 5-mm IES), there were 24, 25, 29, and 32 deflections for tissue with 1, 2, 4, and 6 lines of scar, respectively.

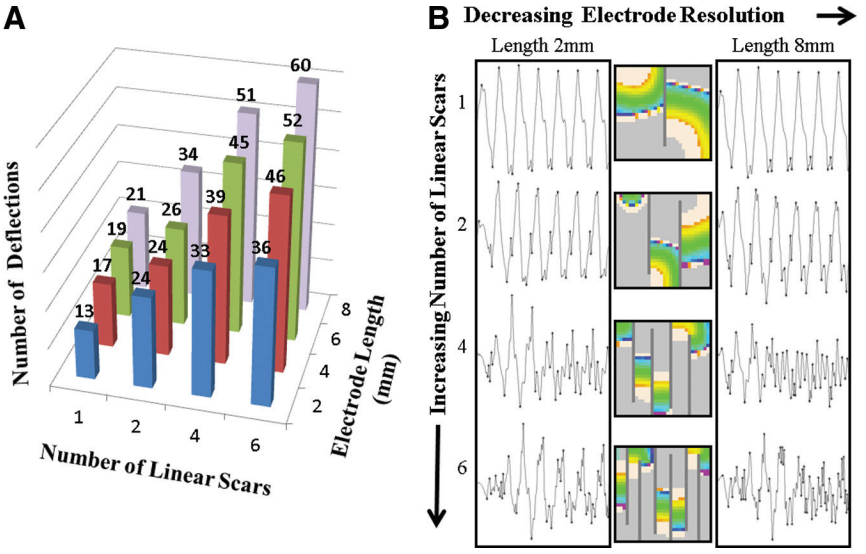

Figure 4. Spatiotemporal variation: electrogram fractionation is dependent on electrode resolution. **A**, Graph of number of deflections in unipolar recordings as a function of spatiotemporal variation (no. of scars) and electrode resolution (length; diameter 1 mm, height 0.5 mm). **B**, Examples of virtual electrograms from tissue stimulated every 150 ms with increasing spatiotemporal variation (1 scar [top] to 6 scars [bottom]) recorded with a unipolar electrode (length 2 mm [left] and 8 mm [right]). Note that number of deflections increases with decreased electrode resolution (effect is more prominent as no. of scars increases).

Table 1. Fractionation Varies With Electrode Characteristics: Tissue With Spatiotemporal Variation*

Unipolar electrode length				
	2 mm	4 mm	6 mm	8 mm
	36	46	52	60
Unipolar electrode diameter				
	1 mm	2 mm	3 mm	4 mm
	52	66	74	76
Unipolar electrode height				
	0.5 mm	1 mm	2 mm	3 mm
	52	68	76	84
Bipolar interelectrode spacing				
	1 mm	3 mm	5 mm	7 mm
	22	24	32	33

*No. of deflections recorded with electrodes of different characteristics in tissue with spatiotemporal variation (zig-zag activation pattern—6 lines of scar). Note that fractionation increases as spatial resolution decreases. Unipolar electrode: 6 mm length, 1 mm diameter and 0.5 mm height (unless specified). Bipolar electrode: 1-mm length and diameter, 0.5-mm height.

Table 2. Fractionation Varies With Interelectrode Spacing: Patients With Atrial Fibrillation

ICL average±SEs		
10-Pole Catheter		
2 mm	9 mm	13 mm
5.2±1.0	8.7±1.0 ($P<0.001$)	9.5±1.0 ($P<0.001$)
20-Pole Catheter		
1 mm	5 mm	7 mm
6.8±1.0	9.9±1.0 ($P<0.001$)	10.3±1.0 ($P<0.001$)
AIPI averages±SEs		
10-Pole Catheter		
2 mm	9 mm	13 mm
207±19	116±19 ($P<0.001$)	106±19 ($P<0.001$)
20-Pole Catheter		
1 mm	5 mm	7 mm
144±13	99±13 ($P<0.001$)	92±13 ($P<0.001$)

ICL and AIPI recorded from coronary sinus of patients during atrial fibrillation. Average values presented for 10-pole and 20-pole catheter as interelectrode spacing increases.

ICL indicates interval confidence length; AIPI, average interpotential interval.

Impact of Electrode Spatial Resolution—Spatiotemporal Variation

In the setting of spatiotemporal variation (cycle length 150 ms, varied number of scars), the number of turning points increased in proportion to unipolar length (diameter 1 mm and height 0.5 mm) and number of linear scars (Figure 4; Table 1). In tissue with 6 lines of scar, the number of deflections was proportional to electrode diameter: 52, 66, 74, and 76 deflections for electrodes of 1-, 2-, 3-, and 4-mm diameter, respectively (length 6 mm and height 1 mm). With constant electrode size (length 6 mm and diameter 1 mm), the number of deflections was directly proportional to electrode height: 52, 68, 76, and 84 deflections at heights of 0.5, 1, 2, and 3 mm above the tissue, respectively. Fractionation also increased with increasing IES: 22, 24, 32, and 33 deflections for IES 1, 3, 5, and 7 mm, respectively (1-mm length and diameter, 0.5-mm height).

Clinical Studies

Complex Fractionated Atrial Electrogram and Spatial Resolution

Qualitatively the effect of interelectrode spacing on spatial resolution (in sinus rhythm) and fractionation (during AF) is easily appreciated (Figure 5). To quantify the effects of spatial resolution on complex fractionated atrial electrogram, we measured ICL and AIPI as a function of IES during AF. Fractionation increased with increasing IES (Table 2). Average values (and SEs) were as follows: ICL 10-pole catheter: 5.2±1.0, 8.7±1.0, and 9.5±1.0 for 2, 9, and 13 mm IES, respectively ($P<0.001$, 2 versus 9 and 2 versus 13 mm); 20-pole catheter: AIPI confidence level 6.8±1.0, 9.9±1.0, and 10.3±1.0 for 1, 5, and 7 mm IES, respectively ($P<0.001$ 1 versus 5 mm and 1 versus 7 mm). AIPI decreased with increased IES—10-pole catheter: 207±19, 116±19, and 106±19 for 2, 9, and 13 mm IES, respectively ($P<0.001$, 2 versus 9 mm and 2 versus 13 mm); AIPI 20-pole catheter: 144±13, 99±13, and 92±13 ($P<0.001$, 1 versus 5 mm and 1 versus 7 mm). As IES increases, electrodes record signals from locations that are progressively farther apart and are therefore exposed to different electromagnetic noise. Bipolar recordings reflect only the difference between the signals recorded at each electrode; therefore, as the difference in noise recorded at each electrode becomes greater, the amplitude of noise in the bipolar signal becomes larger. As a result,

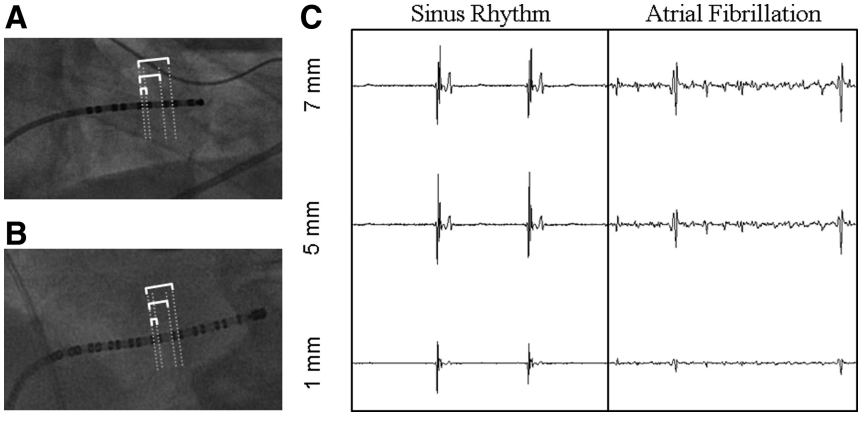

Figure 5. Impact of interelectrode spacing on electrograms recorded in the coronary sinus during sinus rhythm and atrial fibrillation. **A**, Fluoroscopic image of 10-pole catheter in the coronary sinus (electrode length 2 mm, interelectrode spacing 2–5-2 mm). Brackets indicate interelectrode spacings used for reconstruction of bipolar recordings. **B**, Fluoroscopic image of 20-pole catheter (electrode length 1 mm, interelectrode spacing 1–3-1 mm). **C**, Simultaneous electrogram recordings (IES as indicated). Note minor increase in baseline noise as IES increases (sinus rhythm) and increased fractionation with increased IES (atrial fibrillation). IES indicates interelectrode spacing.

one can expect that noise is progressively increased as IES increases. We measured noise as a function of IES; the mean amplitude of noise increased with IES but remained <0.05 mV (maximum 0.028 ± 0.01 mV).

Discussion

The fact that electrodes measure electric potential rather than tissue current density creates a possible source of ambiguity in the interpretation of electrograms. Because currents generate a potential field that spreads through space (with amplitude that decreases with distance),[10,20] potential recordings at any site reflect contributions from current sources at multiple sites. This capacity for "far-field" recording has the result that electrogram deflections occur with variation of current density over an area larger than the physical dimensions of the electrode. Electrogram fractionation is generally defined as low-amplitude, high-frequency deflections. As the number of sites contributing to an electrode's potential increases, the number of deflections will increase so long as these sites are excited asynchronously. When sites are excited simultaneously, their impact on the electrogram amplitude is additive but fractionation does not result.

In our study, we used a simple model to independently control each of the components that contribute to fractionation: tissue spatiotemporal variation, tissue temporal variation, and electrode spatial resolution. We made the following observations: (1) fractionation is not observed with spatial variation alone; secondary to temporal superposition, the contributions from spatially disparate currents to the potential recorded at any electrode location sum to alter amplitude without producing fractionation; (2) fractionation is observed with temporal variation, which is independent of electrode spatial resolution; and (3) fractionation is observed with spatiotemporal variation and in this case is dependent on electrode spatial resolution. Consequently, spatial resolution determines the limit of the ability to distinguish temporal from spatiotemporal variation; that is, increased frequency as a result of overcounting.

Relationship to Previous Studies

Gardner et al found that fractionated ventricular electrograms in the setting of postinfract scar results from local dissociation of activation timing between closely spaced muscle bundles separated by fibrous scar.[15] Although their study did not directly assess the relationship between spatial resolution and fractionation, their conclusions were based on comparison of macroscopic recordings (0.3-mm diameter, 0.5–1.0 mm IES) with microscopic recordings (1–5 μm tip, unipolar) and were confirmed with histological examination. de Bakker et al meticulously demonstrated that "zig-zag" conduction through a "complex network of connected tracts" results in electrogram fractionation in superfused infarcted human papillary muscle.[26] By placing a linear array of high-resolution electrodes (100-μm silver chloride wire) oriented perpendicularly to fiber direction, they were able to demonstrate sequential (asynchronous) activation of between 2 and 35 interconnected fibers. Although they did not systematically examine the relationship between tissue variation and spatial resolution, Jacquemet and Henriquez created a computer model of microfibrosis in which fractionation varied directly with the density of "collagenous" septa and increased when a larger electrode was used.[22] The same results were obtained in a computer model of electric conduction in a study performed by Lesh et al.[16] Kalifa and colleagues demonstrated fractionation at the junction between rapid organized rotors and the surrounding area where wavebreak produced variable conduction patterns.[13] Furthermore, it has been demonstrated in computer models, isolated sheep hearts, and monolayers of murine atrial myocytes[11,12] that a meandering rotor generates electrogram fractionation. The common feature in all of these studies is the presence of multiple discretely and asynchronously activating muscle bundles.

To our knowledge, the present study is the first to explicitly and systematically explore and characterize the relationship among tissue spatiotemporal activation, electrode resolution, and electrogram fractionation.

Limitations

Our computer model makes no attempt to reproduce the specific functional and anatomic features of tissue excitation patterns. As a result, our electrograms do not mimic clinically recorded fractionated signals. It was not our intention to investigate the mechanism of any specific instance of physiological fractionation. Instead, our goal was to establish which parameters contribute to fractionation in general and to determine how these parameters interact to produce fractionation. With the use of a simple model, the roles of individual parameters could be independently examined. Our findings are commensurate with a large body of physiological recordings of fractionation resulting from varied activation patterns. We confirmed the general principles elucidated by our computer model in patients with AF. In the clinical experiments, the role of spatial resolution was measured by varying interelectrode spacing (we did not assess the impact of electrode size). We chose IES and not size to vary resolution at the same time as holding tissue spatiotemporal variation fixed. To reduce the confounding influence of spatiotemporal variation during AF, we compared only simultaneous recordings of varied resolution. This was practical only by varying IES, because comparing electrodes of different sizes would have required either sampling from different locations (unacceptable secondary to spatial disparities of tissue variation) or at different times (unacceptable secondary to temporal fluctuation of activation).[27]

Conclusion

Electrogram fractionation results from the interaction of 3 components: tissue temporal variation, tissue spatiotemporal variation, and electrode spatial resolution. In the absence of tissue spatiotemporal variation (ie, temporal variation alone), fractionation is independent of electrode spatial resolution. In a computer model of electrically excitable

tissue with spatiotemporal variation and in patients with AF, fractionation increased with decreasing electrode spatial resolution.

Electrograms measure the average potential field at the surface of an electrode over time. As a consequence, multiple different patterns of tissue activation can generate similar electrograms. Analysis of a single fractionated electrogram does not permit differentiation of temporal versus spatiotemporal tissue variation; therefore, one cannot distinguish high-frequency excitation from overcounting. Electrode spatial resolution must be considered when comparing studies of fractionation.

Acknowledgments

We thank Burton Sobel, MD, and Daniel Lustgarten, MD, PhD, for their kind and insightful help preparing the article.

Source of Funding

This study was supported by a grant from Medtronic.

Disclosures

P.S.S. receives research support from Medtronic, Biosense Webster, and St Jude; and consults for Medtronic and Biosense Webster. J.H.T.B. receives research support from Medtronic.

References

1. Stevenson WG, Weiss JN, Wiener I, Rivitz SM, Nademanee K, Klitzner T, Yeatman L, Josephson M, Wohlgelernter D. Fractionated endocardial electrograms are associated with slow conduction in humans: evidence from pace-mapping. *J Am Coll Cardiol*. 1989;13: 369–376.
2. Brunckhorst CB, Delacretaz E, Soejima K, Jackman WM, Nakagawa H, Kuck KH, Ben-Haim SA, Seifert B, Stevenson WG, Brunckhorst CB, Delacretaz E, Soejima K, Jackman WM, Nakagawa H, Kuck K-H, Ben-Haim SA, Seifert B, Stevenson WG. Ventricular mapping during atrial and right ventricular pacing: relation of electrogram parameters to ventricular tachycardia reentry circuits after myocardial infarction. *J Interv Card Electrophysiol*. 2004;11:183–191.
3. Nademanee K, McKenzie J, Kosar E, Schwab M, Sunsaneewitayakul B, Vasavakul T, Khunnawat C, Ngarmukos T. A new approach for catheter ablation of atrial fibrillation: mapping of the electrophysiologic substrate. *J Am Coll Cardiol*. 2004;43:2044–2053.
4. Di Biase L, Elayi CS, Fahmy TS, Martin DO, Ching CK, Barrett C, Bai R, Patel D, Khaykin Y, Hongo R, Hao S, Beheiry S, Pelargonio G, Dello Russo A, Casella M, Santarelli P, Potenza D, Fanelli R, Massaro R, Wang P, Al-Ahmad A, Arruda M, Themistoclakis S, Bonso A, Rossillo A, Raviele A, Schweikert RA, Burkhardt DJ, Natale A. Atrial fibrillation ablation strategies for paroxysmal patients: randomized comparison between different techniques. *Circ Arrhythm Electrophysiol*. 2009;2: 113–119.
5. Elayi CS, Verma A, Di Biase L, Ching CK, Patel D, Barrett C, Martin D, Rong B, Fahmy TS, Khaykin Y, Hongo R, Hao S, Pelargonio G, Dello Russo A, Casella M, Santarelli P, Potenza D, Fanelli R, Massaro R, Arruda M, Schweikert RA, Natale A. Ablation for longstanding permanent atrial fibrillation: results from a randomized study comparing three different strategies. *Heart Rhythm*. 2008;5:1658–1664.
6. Khaykin Y, Skanes A, Champagne J, Themistoclakis S, Gula L, Rossillo A, Bonso A, Raviele A, Morillo CA, Verma A, Wulffhart Z, Martin DO, Natale A. A randomized controlled trial of the efficacy and safety of electroanatomic circumferential pulmonary vein ablation supplemented by ablation of complex fractionated atrial electrograms versus potential-guided pulmonary vein antrum isolation guided by intracardiac ultrasound. *Circ Arrhythm Electrophysiol*. 2009;2: 481–487.
7. Oral H, Chugh A, Yoshida K, Sarrazin JF, Kuhne M, Crawford T, Chalfoun N, Wells D, Boonyapisit W, Veerareddy S, Billakanty S, Wong WS, Good E, Jongnarangsin K, Pelosi F Jr, Bogun F, Morady F. A randomized assessment of the incremental role of ablation of complex fractionated atrial electrograms after antral pulmonary vein isolation for long-lasting persistent atrial fibrillation. *J Am Coll Cardiol*. 2009;53: 782–789.
8. Li W-J, Bai Y-Y, Zhang H-Y, Tang R-B, Miao C-L, Sang C-H, Yin X-D, Dong J-Z, Ma C-S. Additional ablation of complex fractionated atrial electrograms after pulmonary vein isolation in patients with atrial fibrillation/clinical perspective. *Circ Arrhythm Electrophysiol*. 2011;4: 143–148.
9. Porter M, Spear W, Akar JG, Helms R, Brysiewicz N, Santucci P, Wilber DJ. Prospective study of atrial fibrillation termination during ablation guided by automated detection of fractionated electrograms. *J Cardiovasc Electrophysiol*. 2008;19:613–620.
10. Kootsey JM, Johnson EA. Origin of the electrocardiogram: relationship between transmembrane potential and the electrocardiogram. In: Nelson CV, Geselowitz DB, eds. *Theoretical Basis of Electrocardiology*. London: Oxford University Press; 1976:21–43.
11. Umapathy K, Masse S, Kolodziejska K, Veenhuyzen GD, Chauhan VS, Husain M, Farid T, Downar E, Sevaptsidis E, Nanthakumar K. Electrogram fractionation in murine HL-1 atrial monolayer model. *Heart Rhythm*. 2008;5:1029–1035.
12. Zlochiver S, Yamazaki M, Kalifa J, Berenfeld O. Rotor meandering contributes to irregularity in electrograms during atrial fibrillation. *Heart Rhythm*. 2008;5:846–854.
13. Kalifa J, Tanaka K, Zaitsev AV, Warren M, Vaidyanathan R, Auerbach D, Pandit S, Vikstrom KL, Ploutz-Snyder R, Talkachou A, Atienza F, Guiraudon G, Jalife J, Berenfeld O. Mechanisms of wave fractionation at boundaries of high-frequency excitation in the posterior left atrium of the isolated sheep heart during atrial fibrillation. *Circulation*. 2006;113: 626–633.
14. Berenfeld O, Zaitsev AV, Mironov SF, Pertsov AM, Jalife J. Frequency-dependent breakdown of wave propagation into fibrillatory conduction across the pectinate muscle network in the isolated sheep right atrium. *Circ Res*. 2002;90:1173–1180.
15. Gardner PI, Ursell PC, Fenoglio JJ Jr, Wit AL. Electrophysiologic and anatomic basis for fractionated electrograms recorded from healed myocardial infarcts. *Circulation*. 1985;72:596–611.
16. Lesh MD, Spear JF, Simson MB. A computer model of the electrogram: what causes fractionation? *J Electrocardiol*. 1988;21(suppl): S69–S73.
17. Narayan SM, Wright M, Derval N, Jadidi A, Forclaz A, Nault I, Miyazaki S, Sacher F, Bordachar P, Clementy J, Jais P, Haissaguerre M, Hocini M. Classifying fractionated electrograms in human atrial fibrillation using monophasic action potentials and activation mapping: evidence for localized drivers, rate acceleration, and nonlocal signal etiologies. *Heart Rhythm*. 2011;8:244–253.
18. Durrer D, Van Der Tweel LH. Excitation of the left ventricular wall of the dog and goat. *Ann N Y Acad Sci*. 1957;65:779–803.
19. Spector PS, Habel N, Sobel BE, Bates JH, Spector PS, Habel N, Sobel BE, Bates JHT. Emergence of complex behavior: an interactive model of cardiac excitation provides a powerful tool for understanding electric propagation. *Circ Arrhythm Electrophysiol*. 2011;4:586–591.
20. Plonsey R, Barr RC. *Sources and Fields. Bioelectricity. A Quantitative Approach,* 3rd ed: New York, Springer; 2007:23–42.
21. Lellouche N, Buch E, Celigoj A, Siegerman C, Cesario D, De Diego C, Mahajan A, Boyle NG, Wiener I, Garfinkel A, Shivkumar K. Functional characterization of atrial electrograms in sinus rhythm delineates sites of parasympathetic innervation in patients with paroxysmal atrial fibrillation. *J Am Coll Cardiol*. 2007;50:1324–1331.
22. Jacquemet V. Genesis of complex fractionated atrial electrograms in zones of slow conduction: a computer model of microfibrosis. *Heart Rhythm*. 2009;6:803–810.
23. Scherr D, Dalal D, Cheema A, Nazarian S, Almasry I, Bilchick K, Cheng A, Henrikson CA, Spragg D, Marine JE, Berger RD, Calkins H, Dong J. Long- and short-term temporal stability of complex fractionated atrial electrograms in human left atrium during atrial fibrillation. *J Cardiovasc Electrophysiol*. 2008;20:13–21.
24. Scherr D, Dalal D, Cheema A, Cheng A, Henrikson CA, Spragg D, Marine JE, Berger RD, Calkins H, Dong J. Automated detection and characterization of complex fractionated atrial electrograms in human left atrium during atrial fibrillation. *Heart Rhythm*. 2007;4: 1013–1020.

25. Nademanee K, Schwab M, Porath J, Abbo A. How to perform electrogram-guided atrial fibrillation ablation. *Heart Rhythm*. 2006;3: 981–984.
26. de Bakker JM, van Capelle FJ, Janse MJ, Tasseron S, Vermeulen JT, de Jonge N, Lahpor JR. Slow conduction in the infarcted human heart. 'zigzag' course of activation. *Circulation*. 1993;88:915–926.
27. Habel N, Znojkiewicz P, Thompson N, Müller JG, Mason B, Calame J, Calame S, Sharma S, Mirchandani G, Janks D, Bates J, Noori A, Karnbach A, Lustgarten DL, Sobel BE, Spector P. The temporal variability of dominant frequency and complex fractionated atrial electrograms constrains the validity of sequential mapping in human atrial fibrillation. *Heart Rhythm*. 2010;7:586–593.

CLINICAL PERSPECTIVE

In this article we describe the relationship among tissue spatiotemporal variation, electrode spatial resolution, and electrogram fractionation. The clinically relevant point to be noted is that although as clinicians we are interested in measuring the distribution of current in the cardiac tissue, we measure the potential field above the tissue. Because all tissue currents contribute to the potential field that surrounds the heart, the potential at any particular location reflects local and remote currents. When the electric activity in the heart is spatially and temporally complex (eg, fibrillation), electrogram measurements become fractionated. This fractionation is proportional to the size of the electrode recording area, that is, the spatial resolution. Therefore, electrogram fractionation varies not only with tissue electric activity, but also depends on the properties of the recording electrode(s).